Proceedings of the 2018 IEEE/ASME International
Conference on Advanced Intelligent Mechatronics (AIM),
Auckland, New Zealand, July 9-12, 2018

Independent Estimation of Temperature and Strain in Tee-Rosette Piezoresistive Strain Sensors*

Meysam Omidbeike[1], Ben Routley[1] and Andrew J. Fleming[1]

***Abstract*— This article proposes a novel technique for independent measurement of strain and temperature in piezoresistive strain sensors configured in a tee-rosette. The most notable property of piezoresistive sensors is their easy integration into MEMS fabrication processes and nanopositioning systems which makes them highly advantageous for both size and cost. The foremost disadvantage associated with piezoresistive sensors is high temperature sensitivity. The proposed estimator allows independent estimation of strain and temperature, which eliminates drift due to temperature variation. Experimental results are presented for motion sensing of a piezoelectric stack actuator which shows a strain measurement with a mean absolute error of 2.16% over a temperature range of -15°C to 40°C.**

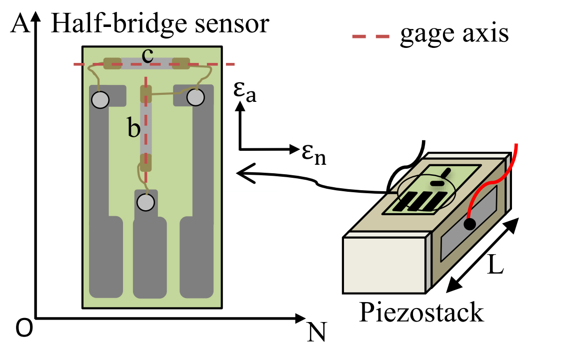

Fig. 1. Tee-rosette half-bridge sensor mounted on a piezostack actuator. Two thermally matched gages a and b are aligned along axes ON and OA respectively. The dashed lines show the axis of each gage.

I. INTRODUCTION

The sensor requirements of a nanopositioning system are among the most demanding of any control system [1]. Due to their high sensitivity and low noise, piezoresistive sensors have been widely used in nanopositioning applications including atomic force microscopy [2]–[5] and nanofabrication [6].

The Wheatstone-bridge is a common configuration for strain gage sensors. In this configuration, the output voltage difference is proportional to the strain experienced by the sensors in each arm of the bridge [7]. In applications that involve equal extension and contraction of the surface area, full or half-bridge configurations are preferred.

The foremost difficulty with piezoresistive sensors is the high temperature sensitivity of both the total resistance and gage factor, described by the TCR (Temperature coefficient of resistance) and TCGF (Temperature coefficient of gage factor). Due to the variation of the gage factor, standard approaches to temperature compensation, such as the unstrained sensor method [8], are not effective.

A number of electrical methods have been proposed for temperature compensation in piezoresistive sensors [9], [10]. However, these methods require equal and opposite strains, such as that found on the top and bottom of a bending beam. The smart sensor proposed in reference [11] uses a thin film thermocouple for temperature measurement. In this method, three different sensing technologies including thermocouple, strain gage and heat flux gage were integrated into a single, multifunctional gage. This configuration provides separate temperature, strain and heat flux measurements, however extensive calibration is required.

The separate measurement of strain and temperature was reported in reference [12]. In this technique, two sensors fabricated from different sensing materials were placed in close vicinity to each other. This temperature and strain are determined from the differing response of each material; however, this method can not be applied to piezoresistive sensors due to temperature sensitivity of the gage factor. In this paper, a novel technique is described for estimating the strain and temperature in a piezoresistive half-bridge arranged in a 90-degree tee rosette. This method is ideal for applications where only positive strain is produced, for example, in piezoelectric stack actuators. The proposed method is demonstrated by measuring the position of a piezoelectric stack actuator subjected to temperature variation.

II. Piezoresistive Sensor Modelling

As illustrated in Fig. 1, the tee-rosette piezoresistive sensor used in the proposed design consists of two thermally matched gages bonded to a backing material. To model the resistance change in each gage, a single pizoresitive strain gage subjected to a biaxial strain field is considered first. When a gage is subjected to strains parallel and normal to the gage axis, the total change in resistance can be written as [13]

$$\Delta R = \Delta R_a + \Delta R_n, \tag{1}$$

where ΔR_a is a change in resistance due to the axial strain and ΔR_n is a change in resistance due to the normal strain. Each term on the right-hand side of Eq. (1) can be expressed

*Supported by the Australian Research Council Grants DP150103521, FT130100543, and DP120100487.

[1]The authors are with the School of Electrical Engineering and Computer Science, University of Newcastle, Australia
meysam.omidbeike@uon.edu.au
andrew.fleming@newcastle.edu.au

978-1-5386-1854-7/18/$31.00 ©2018 IEEE

by the general strain gage equation given by

$$\Delta R = S\epsilon\bar{R}, \tag{2}$$

where S is strain sensitivity, ϵ is applied strain and $\bar{R}$ is nominal resistance. By substituting Eq. (2) into Eq. (1), the following equation is found

$$\Delta R = S_a\epsilon_a\bar{R} + S_n\epsilon_n\bar{R}, \tag{3}$$

where S_a is the axial strain sensitivity, S_n is the normal strain sensitivity, ϵ_a is the axial strain and ϵ_n is the normal strain applied to the sensor. As the sensor specifications typically include the gage factor (determined under uniaxial strain field) and the transverse sensitivity factor, Eq. (3) needs to be written in terms of these two quantities. This can be done by rewriting Eq. (3) as

$$\Delta R = S_a\bar{R}(\epsilon_a + \frac{S_n}{S_a}\epsilon_n). \tag{4}$$

Here, the ratio S_n/S_a is known as the transverse sensitivity factor, represented by the symbol K, and S_a is the axial strain sensitivity identical to the manufacturer's gage factor G_F [13].

Since the sensors are matched, they have equal strain sensitivity and transverse sensitivity factor. However, there is a 90 degree offset between each axis which results in different strain conditions for each of the sensors. Fig. 1 shows the configuration of each sensor with respect to the reference axes OA and ON. Here it can be seen that the strain condition for sensor b is such that strain ϵ_a is parallel to the gage axis, while ϵ_n is normal to the gage axis. The strain condition for sensor c is the opposite. By considering this and using Eq. (3), the total resistance change in each sensor can be written as

$$\Delta R_b = \epsilon_a S_a\bar{R}_b + \epsilon_n S_n\bar{R}_b \tag{5}$$

$$\Delta R_c = \epsilon_n S_a\bar{R}_c + \epsilon_a S_n\bar{R}_c, \tag{6}$$

where $\bar{R}_b$ is the nominal gage resistance of sensor b and $\bar{R}_c$ is the nominal gage resistance of sensor c. Expressing ΔR_b as $R_b - \bar{R}_b$ and rearranging for R_b, and similarly for ΔR_c, Eq. (5) and Eq. (6) becomes

$$R_b = \bar{R}_b + \epsilon_a S_a\bar{R}_b - \epsilon_n S_n\bar{R}_b \tag{7}$$

$$R_c = \bar{R}_c + \epsilon_n S_a\bar{R}_c + \epsilon_a S_a\bar{R}_c, \tag{8}$$

In order to estimate temperature and strain independently, Eq. (7) and Eq. (8) are solved simultaneously for ϵ_a and T. Using the transverse sensitivity factor $K = S_n/S_a$ and Poisson's ratio $\nu = -\epsilon_n/\epsilon_a$, Eq. (7) and Eq. (8) can be written as a function of gage factor $G_F = S_a$ and axial strain ϵ_a

$$R_b = \bar{R}_b + \epsilon_a G_F\bar{R}_b - \nu\epsilon_a K G_F\bar{R}_b \tag{9}$$

$$R_c = \bar{R}_c - \nu\epsilon_a G_F\bar{R}_c + \epsilon_a K G_F\bar{R}_b. \tag{10}$$

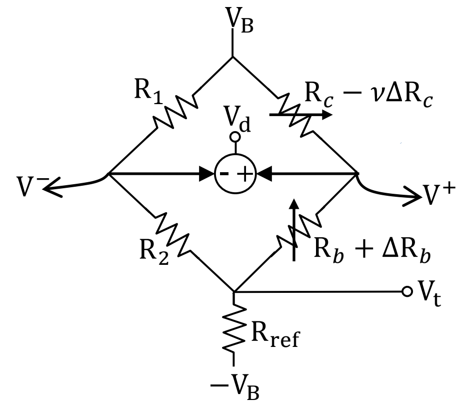

Fig. 2. Schematic of the circuit for real-time resistance readings of sensors b and c.

The linear temperature dependency of gage factor G_F and resistance R can be expressed by

$$G_F(T) = G_F(1 + \beta\Delta T) \tag{11}$$

$$R(T) = \bar{R}(1 + \alpha\Delta T), \tag{12}$$

where β is the temperature coefficient of gage factor (TCGF) and α is the temperature coefficient of resistance (TCR). Including first order temperature variation into Eq. (9) and Eq. (10) gives,

$$\begin{aligned} R_b(\epsilon_a, T) = \bar{R}_b(1 + \alpha\Delta T)[&\epsilon_a G_F(1 + \beta\Delta T) \\ &- \nu\epsilon_a K G_F(1 + \beta\Delta T)] \end{aligned} \tag{15}$$

and

$$\begin{aligned} R_c(\epsilon_a, T) = \bar{R}_c(1 + \alpha\Delta T)[&\epsilon_a K G_F(1 + \beta\Delta T) \\ &- \nu\epsilon_a G_F(1 + \beta\Delta T)] \end{aligned} \tag{16}$$

where ν_0 is the Poisson's ratio, K is the transverse sensitivity factor, ϵ_a is the strain in the axial direction, and G_F is the gage factor. With two strain sensors in a tee-rosette configuration, a system of two equations has been created which can be simultaneously solved for strain and temperature. The resulting independent equations for $\hat{T}$ and $\hat{\epsilon}_a$ are given in Eq. (13) and Eq. (14). Both equations are functions of two variables R_a and R_b, plus the sensor characteristic constants α, β, K, G_F, ν, $\bar{R}_b$ and $\bar{R}_c$.

III. Requirements for Independent Strain And Temperature Measurement

The real time measurement of strain and temperature requires sensor resistances to be read online. The resistance readings have been performed using the full-bridge configuration shown in Fig. 2. Deriving two equations for the voltages V_d and V_t allows the sensor resistances to be determined by solving two equations simultaneously. This gives

$$R_a(V_t, V_d) = \frac{R_{ref}(R_2(V_B - V_t) + V_d(R_1 + R_2)}{V_B(R_1 + R_2) + R_{ref}(V_t - V_B) \atop {}_1 \qquad\qquad + V_t(R_1 + R_2)} \tag{17}$$

$$\widehat{T}(R_b,R_c)=\frac{\begin{array}{c}\bar{R}_b\bar{R}_c-\bar{R}_bR_c-K\bar{R}_b\bar{R}_c+K\bar{R}_bR_b+\bar{R}_b\bar{R}_c\nu-\bar{R}_cR_c\nu-\bar{R}_b\bar{R}_cT_0\alpha\\-K\bar{R}_b\bar{R}_c\nu+K\bar{R}_bR_b\nu+K\bar{R}_b\bar{R}_cT_0\alpha-\bar{R}_b\bar{R}_cT_0\alpha\nu+K\bar{R}_b\bar{R}_cT_0\alpha\nu\end{array}}{\bar{R}_b\bar{R}_c\alpha(K-\nu+K\nu-1)} \tag{13}$$

$$\widehat{\epsilon}(R_b,R_c)=\frac{(\bar{R}_a\bar{R}_b\alpha(\bar{R}_bR_a-\bar{R}_aR_b)(K-1)(\nu+1))}{\begin{array}{c}(G_F(\bar{R}_bR_c-K\bar{R}_cR_b+\bar{R}_cR_b\nu-K\bar{R}_bR_c\nu)(\beta\bar{R}_b\bar{R}_c+\beta\bar{R}_b\bar{R}_c-\bar{R}_b\bar{R}_c\alpha-\beta K\bar{R}_b\bar{R}_c+\beta K\bar{R}_cR_b\\+K\bar{R}_b\bar{R}_c\alpha+\beta\bar{R}_b\bar{R}_c\nu-\beta\bar{R}_b\bar{R}_cR_b\nu-\bar{R}_b\bar{R}_c\alpha\nu+K\bar{R}_b\bar{R}_c\alpha\nu-\beta K\bar{R}_b\bar{R}_c\nu+\beta K\bar{R}_bR_c\nu))\end{array}} \tag{14}$$

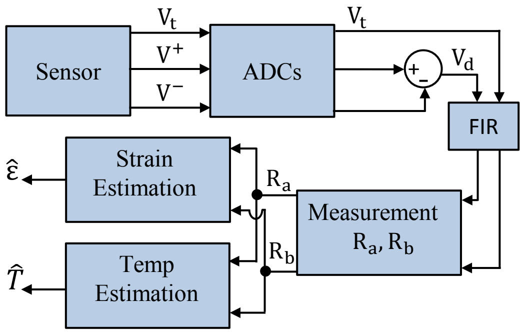

Fig. 3. Data acquisition and signal processing chain of a piezoresistive strain sensor.

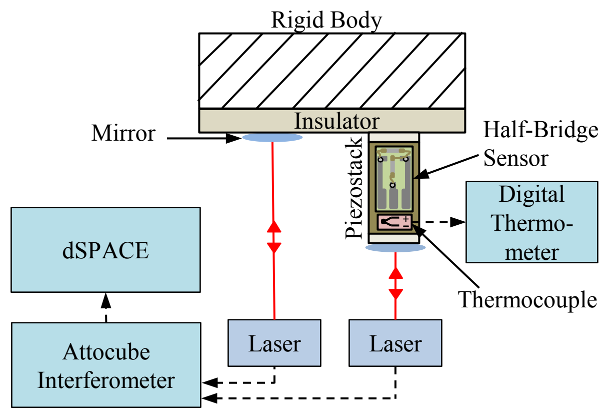

Fig. 4. Experimental set-up for piezoresistive strain sensor calibration.

and

$$R_b(V_t,V_d)=\frac{-R_{ref}(V_d(R_1+R_2)+R_1(V_t-V_B))}{V_B(R_1+R_2)+R_{ref}(V_t-V_B)+V_t(R_1+R_2)} \tag{18}$$

where V_B, R_1, R_2 and R_{ref} are constants. Apart from resistance values, accurate measurement of strain and temperature also requires accurate knowledge of sensor parameters. Due to different thermal expansion coefficients of materials, strain gage sensors will have different characteristic parameters after being bonded on the specimen. Therefore, a calibration experiment must be performed initially to identify the parameters including α (TCR), β (TCGF) and gage factor G_F.

Local optimization techniques can be used to identify the set of model parameters that minimize error between the estimated and true measured value. As the optimization process seeks a point that is locally optimal, the quality of th initial guess can critically affect the solution [14]. Therefore, an initial calibration procedure is proposed to identify a suitable starting point for the optimization process.

IV. Implementation and Initial Calibration

The proposed technique is demonstrated on a half-bridge piezoresistive sensor bonded to the 150V piezoelectric stack actuator shown in Fig. 1. The block diagram shown in Fig. 3 illustrates the data acquisition process, in addition to the basic input/output structure of the sensor. The real-time data acquisition process was performed by Matlab/Simulink software utilizing a dSPACE DS1103 board. In this process, the voltage readings from the bridge circuit were converted to a discrete time format using three analog to digital converters with a 1-kHz sampling rate. Following the ADCs, a moving average FIR filter is used to reduce the quantization and measurement noise. The initial calibration process identifies the parameters describing the sensor characteristics including gage factor, TCR and TCGF. A sketch of the experimental set-up for calibration is shown in Fig. 4, where a laser interferometer and digital thermometer were used for true strain and temperature measurements. A power resistor is used to heat the stack actuator directly. To minimize heat flow, the actuator is glued to an insulator with a low expansion coefficient. Since objects dimensions are a function of temperature, a compensation for induced strain due to thermal expansion is required. A differential measurement by laser interferometer is used for thermal expansion compensation. Simultaneous measurements from the rigid body and the stack actuator provide the true strain measurement due to actuation voltage. This can be expressed as

$$\epsilon_a=\epsilon_p-\epsilon_t, \tag{19}$$

where ϵ_a is the true strain in the axial direction, ϵ_t is the strain due to thermal expansion and ϵ_p is the strain due to the combination of actuation voltage and the thermal expansion. Accurate temperature readings were performed using a K-type thermocouple bonded to the stack actuator. In the calibration process, the stack actuator was driven in the range between 0V to 140V at 10Hz while, depending on the parameters to be calculated, either temperature or strain was held constant. In case of the gage factor, the stack actuator was driven in a range between $20-140$V in a 20V

Parameter	Initial	Optimal
Nominal Resistance, R_a	1033Ω	1378
Nominal Resistance, R_b	970Ω	1357
Poisson's Ratio, ν_0	-0.3	0.6275
Sensitivity ratio, K	0.002	0.0048
Gage Factor, GF_a	92.2	37.79
TCR, α	0.0063	0.057
TCGF, β	-0.02	-0.03

TABLE I
INITIAL AND OPTIMAL VALUES OF PIEZORESISTIVE SENSOR CHARACTERISTIC PARAMETERS.

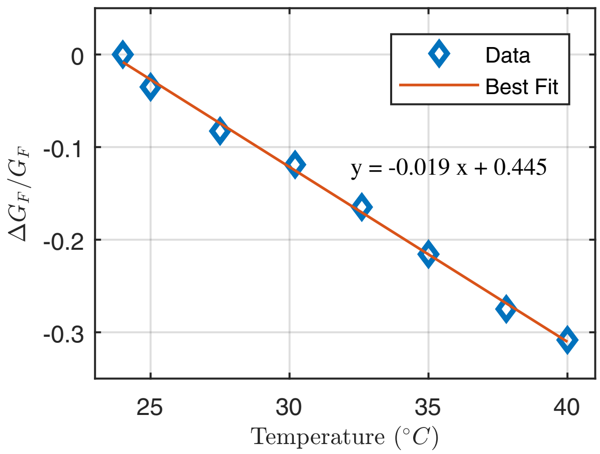

Fig. 5. Temperature coefficient of gage factor. The slope of the best fit line reveals the TCGF value.

steps at 10Hz while the temperature was kept constant at nominal temperature (25°C). In this process, the resistance R_b was recorded and the true strain was measured by the interferometer. The ratio of the fractional change in electrical resistance to the mechanical strain is shown in Fig. 7. Here, the slope of best fit corresponds to the gage factor of the sensor R_b which is 92.2.

For TCGF and TCR calibrations, temperature was varied between nominal 25°C and 45°C while the sensor was held in a constant strain field. The variations in the gage factor and sensor resistance with respect to changes in temperature are shown in Fig. 5 and Fig. 6. Using the slope of best fit, the temperature coefficient of gage factor and the temperature coefficient of resistance were found to be -0.02% and 0.063%, respectively. The parameters of the sensor are summarized in Table I.

V. Piezoresistive Sensor Parameter Identification

A schematic of the piezoresistive sensor is depicted in Fig. 8. Here, R_b and R_c are the inputs, $\hat{\epsilon_a}$ is the output, and θ is the vector of optimization parameters including α, β, G_F, $\bar{R}_b$, $\bar{R}_c$, ν and K.

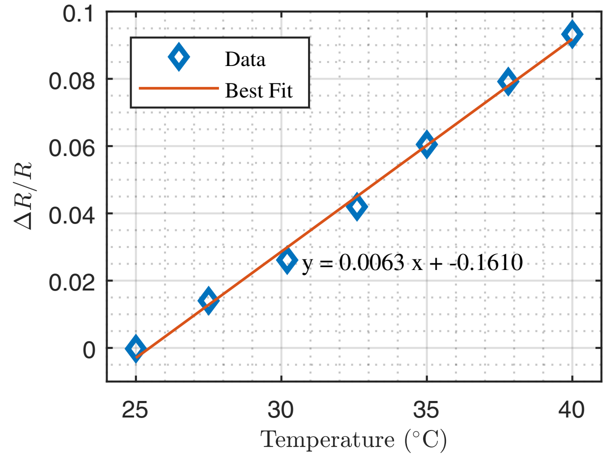

Fig. 6. Temperature coefficient of resistance. The slope of the best fit line reveals the TCR value.

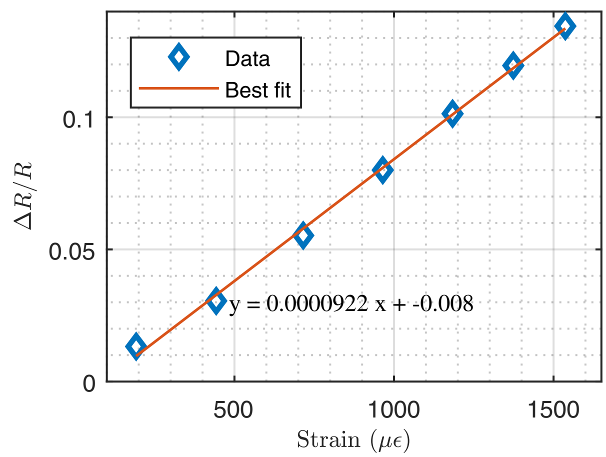

Fig. 7. Resistive response of the sensor b to the applied strain at ambient temperature.

The data set used for the optimization covers both temperature and strain variations. Let Z be the input and output data recorded over a temperature range of $-15°C \le T \le 40°C$:

$$Z = \Big\{[u(T_1), ..., u(T_N)], [y(T_1), ..., y(T_N)]\Big\}, \qquad (20)$$

where

$$u = \Big[\overbrace{[R_b(T_1), ..., R_b(T_N)]}^{R_b}, \overbrace{[R_c(T_1), ..., R_c(T_N)]}^{R_c}\Big] \qquad (21)$$

$$y = \Big[\overbrace{[\hat{\epsilon}_a(T_1), ..., \hat{\epsilon}_a(T_N)]}^{\hat{\epsilon}_a}, \overbrace{[\epsilon_a(T_1), ..., \epsilon_a(T_N)]}^{\epsilon_a}\Big]. \qquad (22)$$

Then the optimization objective is to find a θ that minimizes

$$J(\theta, Z) = ||\epsilon_a - \hat{\epsilon}_a(\theta, u)||_2. \qquad (23)$$

Then the value of θ that minimizes Eq. (23) is

$$\theta = \arg\min_{\theta} J(\theta, Z), \qquad (24)$$

a local solution to this problem is obtained using the Nelder-Mead algorithm [15].

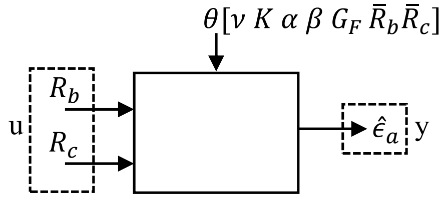

Fig. 8. Schematic of the strain estimation scheme.

	Strain (%)					
	30	40	50	60	70	90
°C	Percentage Error (%)					
−15	5.09	3.21	3.47	0.55	−0.76	2.90
−10	2.37	0.80	1.53	−1.12	−2.13	1.73
−5	0.29	−0.98	0.11	−2.33	−3.09	0.94
0	−1.19	−2.21	−0.80	−3.08	−3.64	0.50
5	−2.13	−2.90	−1.25	−3.40	−3.81	0.41
10	−2.13	−2.90	−1.25	−3.40	−3.59	0.67
15	−2.38	−2.72	−0.75	−2.74	−2.98	1.29
20	−1.69	1.82	0.21	−1.73	−1.96	2.29
25	−2.56	−4.67	−2.70	−4.36	−4.07	0.46
30	−1.43	−3.49	−1.37	−3.02	−2.73	1.90
35	0.80	−1.50	0.54	−1.04	−0.81	3.61
40	4.49	1.89	3.54	1.82	1.67	5.89

TABLE II

PERCENTAGE ERROR IN THE AXIAL STRAIN MEASUREMENTS OVER A TEMPERATURE RANGE OF -15°C TO 40°C.

VI. SENSOR RESPONSE TO TEMPERATURE AND STRAIN

The optimal parameters of the sensor, found when solving Eq. (24) are summarized in Table I. The resulting errors in the axial strain estimation are shown in Table II. The simulation results show an average mean absolute error of 2.16% over a temperature range of -15°C to 40°C. This is a significant result as no additional circuit is used for temperature compensation.

VII. CONCLUSIONS

the article proposes a new technique for independent estimation of temperature and strain in piezoresistive sensors. From two piezoresistive sensors in a tee-rosette configuration, a system of two linear equations is created that allows independent strain and temperature estimations.

The required data acquisition and initial calibration process were demonstrated. To minimize the error between estimated and true strain, the optimal sensor parameters were found usinga calibration and optimization procedure. The resulting strain estimate shows an average mean absolute error of 2.16% over a temperature range of -15°C to 40°C.

Current work is focused on improving the automation and precision of the calibration procedure by using a temperature controlled environmental chamber.

REFERENCES

[1] Andrew J Fleming and Kam K Leang. *Design, modeling and control of nanopositioning systems*. Springer, 2014.
[2] R Jumpertz, AVD Hart, O Ohlsson, F Saurenbach, and J Schelten. Piezoresistive sensors on afm cantilevers with atomic resolution. *Microelectronic Engineering*, 41:441–444, 1998.
[3] R Linnemann, T Gotszalk, L Hadjiiski, and IW Rangelow. Characterization of a cantilever with an integrated deflection sensor. *Thin Solid Films*, 264(2):159–164, 1995.
[4] Daniel Y Abramovitch, Sean B Andersson, Lucy Y Pao, and Georg Schitter. A tutorial on the mechanisms, dynamics, and control of atomic force microscopes. In *American Control Conference, 2007. ACC'07*, pages 3488–3502. IEEE, 2007.
[5] Srinivasa M Salapaka and Murti V Salapaka. Scanning probe microscopy. *IEEE Control Systems*, 28(2):65–83, 2008.
[6] JA Vicary and MJ Miles. Pushing the boundaries of local oxidation nanolithography: Short timescales and high speeds. *Ultramicroscopy*, 108(10):1120–1123, 2008.
[7] Walter G Jung. *Op Amp applications handbook*. Newnes, 2005.
[8] William N Sharpe. *Springer handbook of experimental solid mechanics*. Springer Science & Business Media, 2008.
[9] Ferran Reverter Cubarsí, Goran Horak, Vedran Bilas, and Manuel Gasulla Forner. Novel and low-cost temperature compensation technique for piezoresistive pressure sensors. In *XIX IMEKO World Congress. Fundamental and Applied Metrology*, pages 2084–2087, 2009.
[10] Zong Yao, Ting Liang, Pinggang Jia, Yingping Hong, Lei Qi, Cheng Lei, Bin Zhang, Wangwang Li, Diya Zhang, and Jijun Xiong. Passive resistor temperature compensation for a high-temperature piezoresistive pressure sensor. *Sensors*, 16(7):1142, 2016.
[11] Lisa C Martin, John D Wrbanek, and Gustave C Fralick. Thin film sensors for surface measurements [in aerospace simulation facilities]. In *Instrumentation in Aerospace Simulation Facilities, 2001. 19th International Congress on ICIASF 2001*, pages 196–203. IEEE, 2001.
[12] Daniel J Lichtenwalner, Aaron E Hydrick, and Angus I Kingon. Flexible thin film temperature and strain sensor array utilizing a novel sensing concept. *Sensors and Actuators A: Physical*, 135(2):593–597, 2007.
[13] William M Murray and William R Miller. *The bonded electrical resistance strain gage: an introduction*. Oxford University Press, 1992.
[14] Stephen Boyd and Lieven Vandenberghe. *Convex optimization*. Cambridge university press, 2004.
[15] Jeffrey C Lagarias, James A Reeds, Margaret H Wright, and Paul E Wright. Convergence properties of the nelder–mead simplex method in low dimensions. *SIAM Journal on optimization*, 9(1):112–147, 1998.